2017

# Level Anticrossing of Impurity States in Semiconductor Nanocrystals

Anvar S. Baimuratov
*ITMO University, St. Petersbourg, Russia*

Ivan D. Rukhlenko
*ITMO University, St. Petersbourg, Russia*

Vadim K. Turkov
*ITMO University, St. Petersbourg, Russia*

Irina Ponomareva
*TMO University, St. Petersburg, Russia*

Mikhail Yu Leonov
*ITMO University, St. Petersbourg, Russia*

***See next page for additional authors***

**Authors**
Anvar S. Baimuratov, Ivan D. Rukhlenko, Vadim K. Turkov, Irina Ponomareva, Mikhail Yu Leonov, Tatiana S. Perova, Kevin Berwick, Alexander V. Baranov, and Anatoly V. Federov

SCIENTIFIC REPORTS

OPEN

SUBJECT AREAS:
ELECTRONIC PROPERTIES AND MATERIALS
QUANTUM DOTS

Received
27 August 2014

Accepted
16 October 2014

Published
5 November 2014

Correspondence and requests for materials should be addressed to A.S.B. (baimuratov.anvar@gmail.com)

# Level Anticrossing of Impurity States in Semiconductor Nanocrystals

Anvar S. Baimuratov[1,2], Ivan D. Rukhlenko[1,2], Vadim K. Turkov[1], Irina O. Ponomareva[1], Mikhail Yu. Leonov[1], Tatiana S. Perova[3], Kevin Berwick[4], Alexander V. Baranov[1] & Anatoly V. Fedorov[1]

[1]ITMO University, 49 Kronverksky Avenue, 197101 Saint Petersburg, Russia, [2]Monash University, Clayton Campus, Victoria 3800, Australia, [3]Trinity College Dublin, The University of Dublin, Dublin 2, Ireland, [4]Dublin Institute of Technology, Dublin 8, Ireland.

**The size dependence of the quantized energies of elementary excitations is an essential feature of quantum nanostructures, underlying most of their applications in science and technology. Here we report on a fundamental property of impurity states in semiconductor nanocrystals that appears to have been overlooked—the anticrossing of energy levels exhibiting different size dependencies. We show that this property is inherent to the energy spectra of charge carriers whose spatial motion is simultaneously affected by the Coulomb potential of the impurity ion and the confining potential of the nanocrystal. The coupling of impurity states, which leads to the anticrossing, can be induced by interactions with elementary excitations residing inside the nanocrystal or an external electromagnetic field. We formulate physical conditions that allow a straightforward interpretation of level anticrossings in the nanocrystal energy spectrum and an accurate estimation of the states' coupling strength.**

Colloidal semiconductor nanocrystals, also known as quantum dots, have unique optical and electronic properties that are controlled by their size, shape and chemical composition[1–5]. Doping of nanocrystals with impurity atoms or ions is another method of tuning their physical properties, giving rise to many useful optical phenomena[6–9]. The presence of various impurities in semiconductor nanocrystals is responsible *e.g.* for the Stark effect[10], the spin Hall effect[11], the Kondo effect[12], giant Zeeman splitting[13], and light-induced spontaneous magnetization[14]. This provides the basis for applications of semiconductor nanocrystals in nano-devices such as transistors[15,16], light-emitting diodes[17], bioimaging labels[18], chemical sensors[19], solar cells[20] and spintronic devices[21].

There are several methods of doping nanocrystals based on two different fabrication strategies: nucleation doping and growth doping[22,23]. Nucleation doping is realized by mixing the dopant and host precursor during nanocrystal formation[24], whereas the growth-doping strategy requires absorption of dopant precursors by the nanocrystal surface, followed by encapsulation of the precursors through overgrowth of an isocrystalline or heterocrystalline shell. The radial position of impurities inside a semiconductor nanocrystal can be controlled by adding the precursors at different stages of the nanocrystal formation[25]. This control can be performed with angstrom precision, enabling extremely fine tuning of the optical and magnetic properties of the nanocrystals[26].

Nanocrystal impurities are studied theoretically using two major approaches, based on the effective mass approximation. The first approach, relying on an exact solution of the Schrödinger equation for a given confining potential, yields the impurity's wave functions and energy spectrum in quadratures[27–29]. The second technique, employing the variational method, allows one to find an approximate solution to the Schrödinger equation as a linear sum of the exact wave functions corresponding to the nanocrystals with and without an impurity[30,31]. Most of the theoretical work based on the effective mass approximation is devoted to studies of size dependencies of the energy levels and binding energies of impurity states in simple nanocrystals[27,29,32]. A few were focused on modifications of energy spectrum by external electric and magnetic fields[33,34], multilayer nanocrystals with different numbers of shells[35,36], and nanocrystals with off-center impurities[37,38].

Since most of the optical properties of doped nanostructures strongly depend on their size, the study of the size dependencies of nanostructure impurity levels is a problem of both fundamental and applied significance. Precise, yet rather complex and time-consuming methods of single quantum-dot spectroscopy[39–41] allows one to resolve this problem experimentally. In this paper, we theoretically show that the simultaneous exposure of charge carriers to the Coulomb and confining potentials results in two different contributions to the size dependence of the nanocrystal energy spectrum. The confining potential ceases to determine the structure of the spectrum with an increase of the nanocrystal size while the Coulomb potential starts to dominate. As a consequence, the

energies of some impurity states can accidentally coincide in nanocrystals of a particular size. By examining the ordering of the energy levels for two limiting cases of small and large spherical nanocrystals, we show that this accidental degeneracy is inherent to doped nanocrystals regardless of their shape and composition. The degeneracy is removed by any interaction between the degenerate states, leading to the anticrossings in the size dependencies of the respective energy levels. Using an illustrative example of electron–phonon interaction, we show how the accidental degeneracy is removed and identify which anticrossings are easiest to interpret experimentally. We also discuss which anticrossings are convenient to use for the estimation of interaction strengths in semiconductor nanocrystals.

## Results

**Energy spectrum of hydrogenic impurity.** Consider a donor hydrogenic impurity in a spherical semiconductor nanocrystal of radius $R$, as shown in Fig. 1(a). The impurity comprises a positive ion of charge $Ze$, which is located at the nanocrystal center and coupled through the Coulomb interaction to an electron of charge $-e$ and effective mass $m_e$. By assuming that the nanocrystal boundary is impenetrable to the electron, one can find the wave functions and energy spectrum of the impurity from the Schrödinger equation

$$\left(-\frac{\hbar^2}{2m_e}\nabla^2+V(\mathbf{r})\right)\Psi(\mathbf{r})=E\Psi(\mathbf{r}), \qquad (1)$$

in which the confining potential is given by

$$V(\mathbf{r})=\begin{cases}-\alpha/r, & r<R\\ \infty & r\geq R\end{cases}, \qquad (2)$$

with $\alpha = Ze^2/\varepsilon_0$ and $\varepsilon_0$ being the low-frequency permittivity of the nanocrystal.

Owing to the spherical symmetry of the confining potential, Eq. (1) allows an analytical solution[27–29] (see Methods), which enables a simple analysis of the absorption and photoluminescence spectra of nanocrystals with donor impurities[42–46]. It is possible, in particular, to estimate the nanocrystal size by finding the number of absorption peaks lying below the fundamental absorption band. The peaks are centered at the energies of the lowest states in the nanocrystal energy spectrum $E_{n,l}$, corresponding to different principal quantum numbers and angular momenta, $n = 1, 2, 3, \ldots$ and $l = 0, 1, 2, \ldots$ A more practical application is the problem of calculating the size of a nanocrystal with a certain number of impurity states within the band gap. For instance, a nanocrystal of radius $R = 9\ r_B$, where $r_B = \hbar^2/(m_e\alpha)$ is the effective Bohr radius, has five impurity states with negative energies $E_{1,0}$, $E_{1,1}$, and $E_{2,0}$ (the state with $l = 1$ is three-fold degenerate), whereas the energies of the rest of its states are positive [see Fig. 1(b)].

To qualitatively understand how the energies and ordering of impurity states depend on the nanocrystal size, we note that the impurity spectrum transforms into the spectrum of an infinitely high potential well without an impurity when $\alpha = 0$, and becomes similar to the hydrogen-like spectrum for $R \gg r_B$. The ordering of energy levels $E^{(0)}_{n,l} = \hbar^2\xi^2_{n,l}\big/(2m_eR^2)$ in the first case, illustrated by Fig. 1(c), is determined by the zeros $\xi_{n,l}$ of the spherical Bessel functions of the first kind $j_l(z)$. The hydrogen-like spectrum, shown in Fig. 1(d), consists of negative- and positive-energy domains[47]: the negative-energy spectrum $E^{(i)}_v = -\mathrm{Ry}/v^2 (v = 1,2,3,\ldots)$, where $\mathrm{Ry} = m_e\alpha^2/(2\hbar^2)$ is the effective Rydberg, is discrete; and the positive-energy spectrum $E^{(i)}(\mathbf{k}) = \mathrm{Ry}\ k^2$ $(k > 0)$ is continuous.

These limiting cases show that impurity centers should exhibit discrete energy spectra which may extend to negative energies. The negative-energy states are absent in small nanocrystals, emerging one by one and growing in numbers with the nanocrystal radius. The emergence is caused by the weakening of spatial confinement and the reduction of kinetic energy of the impurity electron, and its resulting distancing from the ion[29]. The descent of quantum state $(n, l)$ from the positive-energy domain to the negative-energy domain occurs when its energy passes through zero in the nanocrystal of radius

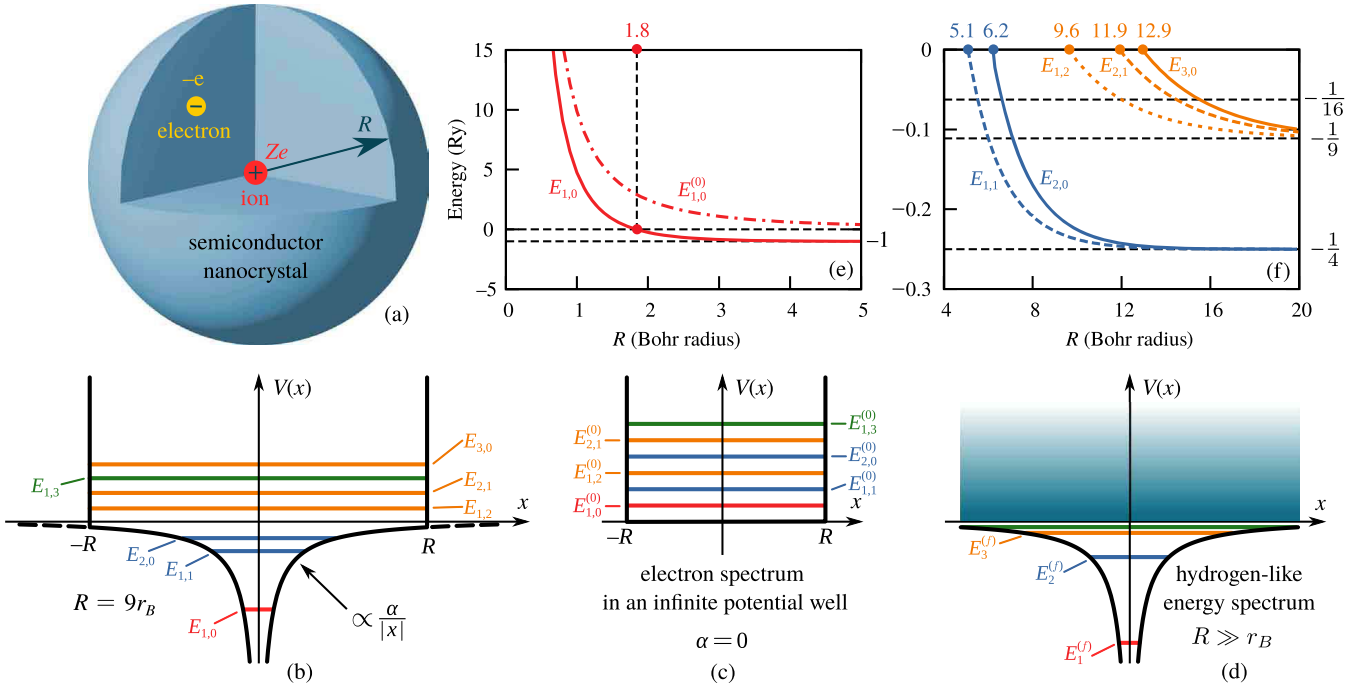


**Figure 1** | (a) Donor impurity at the center of spherical semiconductor nanocrystal of radius $R$; energy spectra of (b) donor impurity for $R = 9\ r_B$, (c) infinitely high spherical potential well without an impurity, and (d) hydrogen-like atom; and size dependencies of energies of (e) first excited and (f) higher impurity states. Dash-dotted curve in (e) is the energy of the lowest state in the potential well.

$$R_{n,l} = \frac{\zeta^2_{n,2l+1}}{8} r_B, \qquad (3)$$

where $\zeta_{n,2l+1}$ is the $n$th zero of the cylindrical Bessel function of the first kind $J_{2l+1}(x)$.

Figures 1(e) and 1(f) show how the energies of the lowest four impurity states vary with $R$. All the energies are seen to be positive for $R < R_{1,0} \approx 1.8\ r_B$. The first state of negative energy appears in the spectrum when the nanocrystal radius exceeds $R_{1,0}$. It is then followed by the higher-energy states with quantum numbers (1, 1), (2, 0), …, and (3, 0), whose energies turn zero for $R \approx 5.1\ r_B$, 6.2 $r_B$, …, and 12.9 $r_B$. As the nanocrystal becomes larger, some of these states start forming multiplets due to the 'accidental' degeneracy of the Coulomb interaction[47]. An unlimited increase in $R$ leads to a transformation of all orbitally nondegenerate impurity states $\{n, l\}$ to hydrogen-like states $\{\nu\}$, which are $\nu$-fold degenerate in angular momentum, so that $E_{n,l} \to E^{(i)}_{n+l} = -\mathrm{Ry}/(n+l)^2$ for $R \to \infty$.

To find the number of negative-energy impurity states in the nanocrystal of radius $R$, one needs to determine the pair of quantum numbers $(n_R, l_R)$ such that $R < \min(R_{n_R,l_R})$. Some algebra shows that there are

$$N(R) = \frac{(n_R + l_R)(n_R + l_R + 1)}{2} - l_R - 1 \qquad (4)$$

states of different energies within the interval $-\mathrm{Ry} \le E_{n,l} < 0$. These states are $(2l+1)$-fold degenerate with respect to the angular momentum projections, making the total number of negative-energy states equal to $(n_R + l_R)(n_R + l_R + 1)(2n_R + 2l_R + 1)/6 - (l_R + 1)^2$. Figure 2(a) shows the staircase function $N(R)$, the steps of which correspond to new negative-energy levels $E_{n_R,l_R}$ successively emerging in the impurity spectrum. The figure enables one to estimate the nanocrystal radius for a known number of negative-energy states, as well as to find the radius required for a desired number of states.

**Anticrossing of impurity energy levels.** Comparison of the impurity spectrum with the spectrum of the nanocrystal without an ion reveals essentially different orderings of their states. This is seen from the order of the first ten levels of the two spectra shown in Fig. 2(b) for $R > R_{4,0}$. By noticing that the ordering of levels $E^{(0)}_{n,l}$ coincides with that in small nanocrystals (with $R \ll r_B$), and recalling that the impurity states form multiplets in large nanocrystals (with $R \gg r_B$), we conclude that the energies of the orbitally nondegenerate impurity states will sometimes coincide as they shift with the nanocrystal radius. Such an 'accidental' degeneracy occurs *e.g.* for a pair of states (2, 0) and (1, 2) in the nanocrystal with $R = 2r_B$. The crossing of the respective energy levels in ZnSe nanocrystals is shown in Fig. 3(a).

Accidental degeneracy resulting from different size dependencies of impurity states is removed by the interaction of the impurity with various excitations of the nanocrystal (phonons[48–51], plasmons[52], excitons[53], *etc.*), external electromagnetic fields[54], or interaction with the environment[55–60]. This causes splitting and anticrossing of the degenerate energy levels. The degree of degeneracy of the impurity states modified by the interaction is determined by the quantum numbers of the initial states and the nature of the interaction. One of the simplest level-anticrossing problems, arising for the lowest-energy accidentally degenerate states (2, 0) and (1, 2), requires solving the sixth-order secular equation. If an interaction of strength $V$ coupling these states does not couple the states of momentum projections $m = 0, \pm 1$, and $\pm 2$, then this equation has three different roots, two of which,

$$\tilde{E}_{\pm} = \frac{1}{2}\left(E_{1,2} + E_{2,0} \pm \sqrt{(E_{1,2} - E_{2,0})^2 + 4V^2}\right), \qquad (5)$$

correspond to nondegenerate states, and one which corresponds to a four-fold degenerate state of energy $E_{1,2}$ (see Methods). Thus the interaction partially removes the six-fold degeneracy of the impurity states at point A. It should be noted that the degeneracy removal in real nanocrystals is always complete due to the existence of coupling between the states of different momentum projections, splitting the four-fold degenerate state into four components.

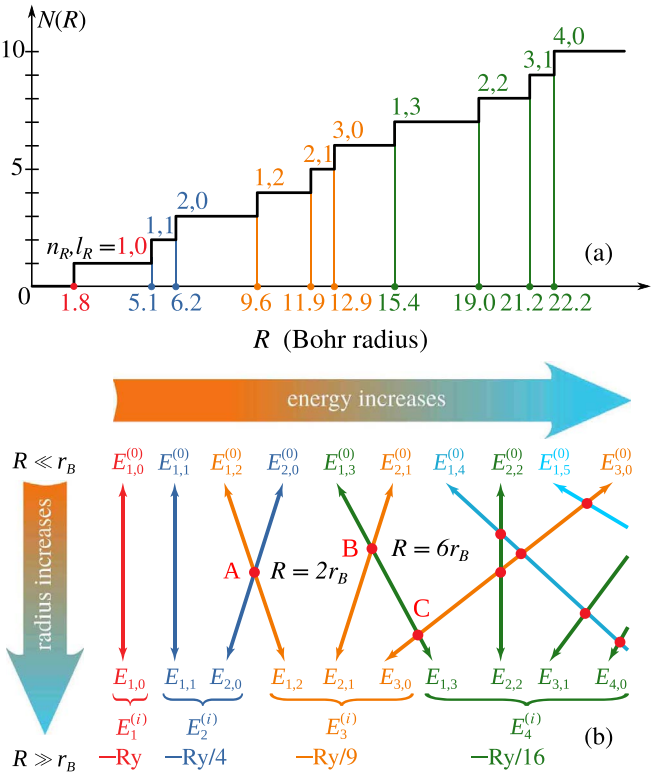


**Figure 2** | (a) Number of negative-energy impurity states *versus* nanocrystal radius $R$ and (b) variation of state ordering with $R$, illustrating formation of accidental-degeneracy points A, B, C, *etc.* in the impurity energy spectrum. Double arrows and underbraces show how the impurity spectrum $E_{n,l}$ (shown for $R > R_{4,0}$) transforms to the hydrogen-like spectrum $E^{(i)}_{n+l}$ when $R \gg r_B$, and to the spectrum of the infinite quantum well without an impurity $E^{(0)}_{n,l}$ when $R \ll r_B$. Note that $E^{(0)}_{n,l} > E_{n,l}$ in an actual energy scale.

Figure 3(b) shows the anticrossing of energy levels $\tilde{E}_+$ and $\tilde{E}_-$, caused by the polar interaction of the states in Fig. 3(a) with dispersionless longitudinal optical (LO) phonons[61–65] confined to the ZnSe nanocrystal. Removal of the accidental degeneracy at point A is seen to result in energy splitting $\tilde{E}_+ - \tilde{E}_- = 2V \approx 13.7$ meV of two out of the six initially degenerate states. This splitting is a natural measure of the electron–LO-phonon interaction strength in the nanocrystal. According to the diagram in Fig. 2(b), the energies $\tilde{E}_+$ and $\tilde{E}_-$ of the split-off states slowly approach Ry/9 $\approx -2.7$ meV and Ry/4 $\approx -6.2$ meV with the increase in the nanocrystal radius.

## Discussion

Strictly speaking, the accidentally degenerate states are coupled by the electron–phonon interaction not only to each other, but also to all other impurity states of the nanocrystal. Since the interaction strength $V$ approximately scales as $\propto R^{-1/2}$ (see Methods) and the energy-level spacing in small nanocrystals grows as $\propto R^{-2}$, the relative contribution of the latter coupling decreases with the reduction of the nanocrystal radius as $\propto R^{3/2}$. This implies that considering a pair of accidentally degenerate states independent of the rest of the nanocrystal states is most justified for states (2, 0) and (1, 2), which are degenerate in the smallest nanocrystal. If an impurity-state level becomes accidentally degenerate several times upon variation of the

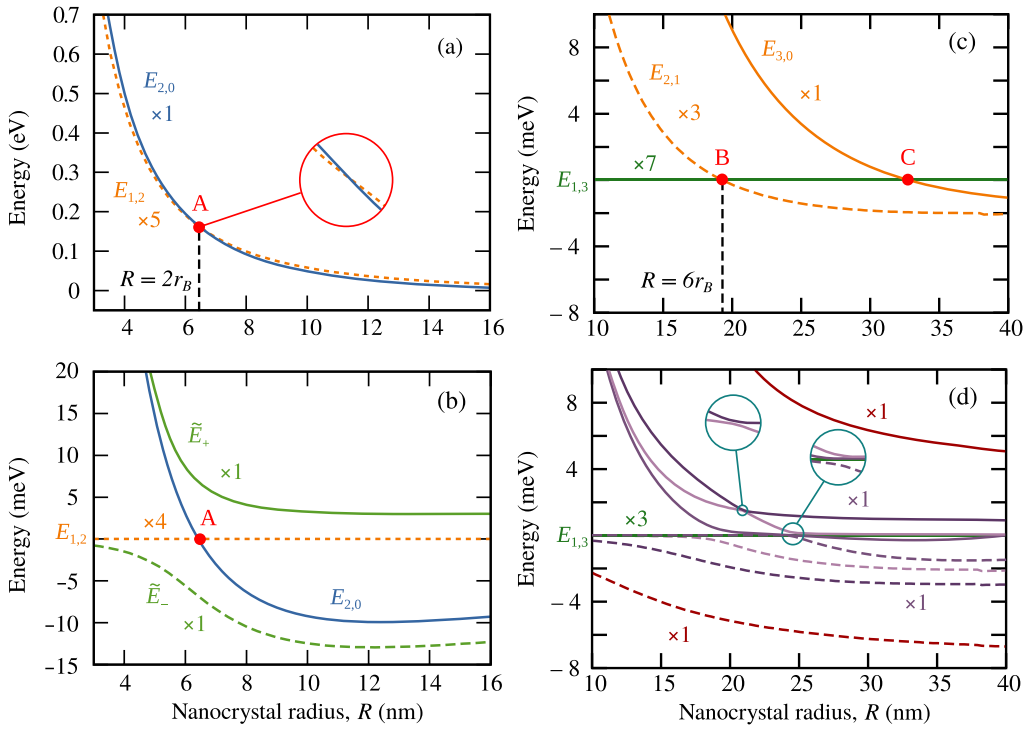


**Figure 3** | (a) Size dependencies of impurity-state energies $E_{1,2}$ and $E_{2,0}$ crossing (see the magnifying inset) at $R = 2r_B \approx 6.4$ nm, and (b) level anticrossing in the presence of electron–LO-phonon interaction. [(c) and (d)] are the same as [(a) and (b)] but for levels $E_{1,3}$, $E_{2,1}$, and $E_{3,0}$. The energies in (b)–(d) are measured from levels $E_{1,2}$ and $E_{1,3}$. For material parameters refer to Methods.

nanocrystal radius, then the resulting anticrossings can be considered independently as long as the interaction of the crossing levels in pairs is much stronger than their interaction with the rest of the impurity levels. Otherwise, an accurate anticrossing description requires taking into account interactions between all the strongly coupled impurity states. This leads to the secular equation of order $\mu = 2(l_1 + l_2 + \cdots + l_\eta) + \eta$, where $l_j$ ($j = 1, 2, \ldots \eta$) are the angular momenta of the strongly coupled states. If $l_z$ is the largest angular momentum and $\mu - 4l_z \geq 2$, then both the accidental degeneracy of the states and their degeneracy in momentum projections are fully removed. The degeneracy removal is partial for $\mu - 4l_z < 2$, with at least one $(4l_z + 2 - \mu)$-fold degenerate impurity state of energy $E_{n_z,l_z}$ left.

Figures 3(c) and 3(d) illustrate the anticrossings of three levels $E_{1,3}$, $E_{2,1}$, and $E_{3,0}$ coupled through the electron–phonon interaction considered earlier. One can see that the interaction leads to a complex anticrossing pattern, which is not the mere sum of two simple patterns similar to those in Fig. 3(b). Since $l_z = 3$ and $\mu = 11$ in this case, the original energy states transform into eight nondegenerate and one three-fold degenerate states. This example shows that only isolated pairs of impurity states that are strongly coupled to each other and weakly coupled to other states are of interest from an experimental viewpoint owing to their simple anticrossing patterns. Since the coupling between nondegenerate impurity states weakens with nanocrystal size, the most 'isolated' anticrossing occurs for states (2, 0) and (1, 2). This anticrossing is the most advantageous for the estimation of the strength of various interactions inside semiconductor nanocrystals.

In conclusion, we have shown that different size dependencies of impurity energy levels in semiconductor nanocrystals result in accidental level degeneracies, the removal of which leads to anticrossings in the size dependencies. Such anticrossings are an important feature inherent to doped nanocrystals, which enables measuring the strength of various interactions of the impurity states with the internal and external elementary excitations of the nanocrystals. We illustrated the removal of the accidental degeneracy of the lowest-energy states by the example of their interaction with optical phonons confined to spherical nanocrystals, and showed that these states are most suited for experimental studies of the nanocrystal anticrossings.

## Methods

**Wave functions and energy spectrum of hydrogenic impurity.** The solution to Eq. (1) is a product of the radial wave function and a spherical harmonic, $\Psi(\mathbf{r}) = F(r)Y_{lm}(\vartheta, \varphi)$, where $r$, $\vartheta$, and $\varphi$ are the spherical coordinates and $l$ and $m$ are the angular momentum and its projection, respectively. Inside the nanocrystal, the radial wave function obeys the equation

$$\frac{\mathrm{d}^2F}{\mathrm{d}r^2} + \frac{2}{r}\frac{\mathrm{d}F}{\mathrm{d}r} - \frac{l(l+1)}{r^2}F + \left(E + \frac{2}{r}\right)F = 0, \tag{6}$$

where radius $r$ and energy $E$ are expressed in units of effective Bohr radius and effective Rydberg constant. The finite solution to this equation at $r = 0$ is proportional to the Kummer function[66] $M(a, b, c)$,

$$F \propto \begin{cases} M(-N+l+1,\ 2l+2,\ 2r/N), & E<0 \\ e^{-iKr}M(i/K+l+1,\ 2l+2,\ 2iKr), & E\geq 0 \end{cases}, \tag{7}$$

where $N = (-E)^{-1/2}$ and $K = E^{1/2}$. The uniform Dirichlet boundary condition $F = 0$ at the nanocrystal surface $r = R$ gives the impurity's energy spectrum

$$E_{nl} = \begin{cases} -1/N_{nl}^2, & E_{nl}<0 \\ K_{nl}^2, & E_{nl}\geq 0 \end{cases}, \tag{8}$$

where $N_{n,l}$ and $K_{n,l}$ are the $n$th positive roots of the equations

$$M(-N_{nl}+l+1,\ 2l+2,\ 2d/N_{nl}) = 0, \tag{9a}$$

$$e^{-iK_{nl}d}M(i/K_{nl}+l+1,\ 2l+2,\ 2iK_{nl}d) = 0, \tag{9b}$$

with $d = R/r_B$. The radial wave function of the impurity states can be finally written as[47]

$$F_{nl} = A_{nl}\left(\frac{r}{R}\right)^l \exp\left(-\frac{c_{nl}r}{2R}\right) M\left(a_{nl}+l+1,\ 2l+2,\ \frac{c_{nl}r}{R}\right), \tag{10}$$

where $A_{nl}$ is the normalization constant, $a_{nl} = -N_{nl}$ and $c_{nl} = -2d/N_{n,l}$ for $E_{nl} < 0$, and $a_{nl} = i/K_{nl}$ and $c_{nl} = 2iK_{nl}d$ for $E_{nl} \geq 0$.

**Degeneracy removal of impurity states.** To determine how a pair of accidentally degenerate impurity states $(n_1, l_1)$ and $(n_2, l_2)$ of energies $E_{n_1,l_1}$ and $E_{n_2,l_2}$ split due to an interaction that does not couple the states differing only by the momentum projections, one needs to solve the secular equation

$$\begin{vmatrix} A_2 & B \\ B^* & A_1 \end{vmatrix} = 0, \tag{11}$$

where $A_j = \left(E_{n_j,l_j} - \tilde{E}\right) I_{l_j}$, $I_l$ is the unit matrix of size $2l + 1$,

$$B = \begin{pmatrix} V^{(q_{11})}_{-l_2;-l_1} & V^{(q_{12})}_{-l_2;-l_1+1} & \cdots & V^{(q_{1,2l_1+1})}_{-l_2;l_1} \\ V^{(q_{21})}_{-l_2+1;-l_1} & V^{(q_{22})}_{-l_2+1;-l_1+1} & \cdots & V^{(q_{2,2l_1+1})}_{-l_2+1;l_1} \\ \vdots & \vdots & \ddots & \vdots \\ V^{(q_{2l_2+1,1})}_{l_2;-l_1} & V^{(q_{2l_2+1,2})}_{l_2;-l_1+1} & \cdots & V^{(q_{2l_2+1,2l_1+1})}_{l_2;l_1} \end{pmatrix} \tag{12}$$

is the $(2l_1 + 1) \times (2l_2 + 1)$ interaction matrix built of matrix elements $V^{(q_{\alpha\beta})}_{m_2;m_1}$, in which $q_{\alpha\beta}$ denotes the quantum numbers of the interaction quasiparticle coupling the states of momentum projections $m_1$ and $m_2$. The $\mu = 2(l_1 + l_2 + 1)$ roots $\tilde{E}_{1(2,3,\ldots,\mu)}$ of Eq. (11), some of which may coincide, are the new energy levels resulting from the splitting. The problem of degeneracy removal for more than two degenerate states is solved in a similar fashion.

The model of longitudinal optical (LO) phonons confined to a spherical semiconductor nanocrystal with a high degree of ionicity yields[61, 64]:

$$V^{(n_q,l_q,m_q)}_{m_2;m_1} = -\sqrt{\frac{(2l_q+1)(2l_1+2)e^2\hbar\Omega}{(2l_2+1)\varepsilon^* R}} C^{l_2 0}_{l_q 0, l_1 0} C^{l_2 m_2}_{l_q m_q, l_1 m_1} \mathcal{I}^{n_q l_q}_{n_2 l_2, n_1 l_1}, \tag{13}$$

where $\varepsilon^* = \varepsilon_0\varepsilon_\infty/(\varepsilon_\infty - \varepsilon_0)$, $\varepsilon_\infty$ and $\varepsilon_0$ are the high- and low-frequency permittivities, $C^{l_2 m_2}_{l_q m_q, l_1 m_1}$ is the Clebsch–Gordan coefficient, and

$$\mathcal{I}^{n_q l_q}_{n_2 l_2, n_1 l_1} = \int_0^R \frac{j_{l_q}\left(\xi_{n_q l_q} x/R\right)}{\xi_{n_q l_q} j_{l_q+1}\left(\xi_{n_q l_q}\right)} F_{n_1 l_1}(x) F_{n_2 l_2}(x) x^2 \mathrm{d}x. \tag{14}$$

Equation (13) shows that the five-fold degenerate impurity state $(1, 2, m)$ is coupled to the nondegenerate impurity state $(2, 0, 0)$ through the five-fold degenerate phonon mode of quantum numbers $(1, 2, m)$. Equation (11) in this case reduces to

$$\left[\left(E_{1,2} - \tilde{E}\right)\left(E_{2,0} - \tilde{E}\right) + V^2\right]\left(E_{1,2} - \tilde{E}\right)^4 = 0, \tag{15}$$

with

$$V^2 = \sum_{m=0,\pm1,\pm2} \left|V^{(1,2,m)}_{0;m}\right|^2. \tag{16}$$

**Material paramseters.** Figure 3 was plotted using Eqs. (13), (14), and (16), by assuming that the nanocrystal is made of ZnSe, and using the following parameters: $Z = 1$, $m_e = 0.15m_0$, $\varepsilon_0 = 9.1$, $\varepsilon_\infty = 6.3$, $\hbar\Omega = 31.7$ meV (the energy of the bulk LO phonon at the Brillouin zone center), $r_B \approx 3.21$ nm, and Ry $\approx 24.6$ meV[67].


1. Baimuratov, A. S. *et al.* Harnessing the shape-induced optical anisotropy of a semi-conductor nanocrystal: A new type of intraband absorption spectroscopy. *J. Phys. Chem. C* **118**, 2867–2876 (2014).
2. Ushakova, E. V. *et al.* Anomalous size-dependent decay of low-energy luminescence from PbS quantum dots in colloidal solution. *ACS Nano* **6**, 8913–8921 (2012).
3. Baimuratov, A. S., Turkov, V. K., Rukhlenko, I. D. & Fedorov, A. V. Shape-induced anisotropy of intraband luminescence from a semiconductor nanocrystal. *Opt. Lett.* **37**, 4645–4647 (2012).
4. Wang, X., Zhuang, J., Peng, Q. & Li, Y. A general strategy for nanocrystal synthesis. *Nature* **437**, 121–124 (2005).
5. Manna, L., Scher, E. C. & Alivisatos, A. P. Synthesis of soluble and processable rod-, arrow-, teardrop-, and tetrapod-shaped CdSe nanocrystals. *J. Am. Chem. Soc.* **122**, 12700–12706 (2000).
6. Koh, W.-K. *et al.* Heavily doped n-type PbSe and PbS nanocrystals using ground-state charge transfer from cobaltocene. *Sci. Rep.* **3**, 2004 (2013).
7. Mocatta, D. *et al.* Heavily doped semiconductor nanocrystal quantum dots. *Science* **332**, 77–81 (2011).
8. Erwin, S. C. *et al.* Doping semiconductor nanocrystals. *Nature* **436**, 91–94 (2006).
9. Shklovskii, B. I. & Efros, A. L. *Electronic Properties of Doped Semiconductors* (Springer-Verlag, New York, 1984).
10. Le Gall, C., Brunetti, A., Boukari, H. & Besombes, L. Optical Stark effect and dressed exciton states in a Mn-doped CdTe quantum dot. *Phys. Rev. Lett.* **107**, 057401 (2011).
11. Tse, W.-K. & Das Sarma, S. Spin Hall effect in doped semiconductor structures. *Phys. Rev. Lett.* **96**, 056601 (2006).
12. Cronenwett, S. M., Oosterkamp, T. H. & Kouwenhoven, L. P. A tunable Kondo effect in quantum dots. *Science* **281**, 540–544 (1998).
13. Yu, J. H. *et al.* Giant Zeeman splitting in nucleation-controlled doped CdSe:Mn quantum nanoribbons. *Nat. Mater.* **9**, 47–53 (2010).
14. Beaulac, R., Schneider, L., Archer, P. I., Bacher, G. & Gamelin, D. R. Light-induced spontaneous magnetization in doped colloidal quantum dots. *Science* **325**, 973–976 (2009).
15. Hetsch, F., Zhao, N., Kershaw, S. V. & Rogach, A. L. Quantum dot field effect transistors. *Mater. Today* **16**, 312–325 (2013).
16. Voznyy, O. *et al.* A charge-orbital balance picture of doping in colloidal quantum dot solids. *ACS Nano* **6**, 8448–8455 (2012).
17. Menkara, H. *et al.* Development of nanophosphors for light emitting diodes. *Opt. Express* **19**, A972–A981 (2011).
18. Wu, P. & Yan, X.-P. Doped quantum dots for chemo/biosensing and bioimaging. *Chem. Soc. Rev.* **42**, 5489–5521 (2013).
19. Thakar, R., Chen, Y. & Snee, P. T. Efficient emission from core/(doped) shell nanoparticles: Applications for chemical sensing. *Nano Lett.* **7**, 3429–3432 (2007).
20. Zhitomirsky, D. *et al.* N-type colloidal-quantum-dot solids for photovoltaics. *Adv. Mater.* **24**, 6181–6185 (2012).
21. Beaulac, R., Archer, P. I., Ochsenbein, S. T. & Gamelin, D. R. Mn-doped CdSe quantum dots: New inorganic materials for spin-electronics and spin-photonics. *Adv. Funct. Mater.* **18**, 3873–3891 (2008).
22. Pradhan, N., Goorskey, D., Thessing, J. & Peng, X. An alternative of CdSe nanocrystal emitters: Pure and tunable impurity emissions in ZnSe nanocrystals. *J. Am. Chem. Soc.* **127**, 17586–17587 (2005).
23. Buonsanti, R. & Milliron, D. J. Chemistry of doped colloidal nanocrystals. *Chem. Mater.* **25**, 1305–1317 (2013).
24. Vlaskin, V. A., Barrows, C. J., Erickson, C. S. & Gamelin, D. R. Nanocrystal diffusion doping. *J. Am. Chem. Soc.* **135**, 14380–14389 (2013).
25. Chen, H.-Y., Maiti, S. & Son, D. H. Doping location-dependent energy transfer dynamics in Mn-doped CdS/ZnS nanocrystals. *ACS Nano* **6**, 583–591 (2012).
26. Yang, Y., Chen, O., Angerhofer, A. & Cao, Y. C. Radial-position-controlled doping in CdS/ZnS core/shell nanocrystals. *J. Am. Chem. Soc.* **128**, 12428–12429 (2006).
27. Ma, L., Zhao, J., Wang, J., Wang, B. & Wang, G. Magnetic properties of transition-metal impurities in silicon quantum dots. *Phys. Rev. B* **75**, 045312 (2007).
28. Hsieh, C.-Y., Chuu, D.-S. & Hsieh, C.-Y. Donor states in a multi-layered quantum dot. *J. Phys.: Condens. Matter* **12**, 8641 (2000).
29. Chuu, D. S., Hsiao, C. M. & Mei, W. N. Hydrogenic impurity states in quantum dots and quantum wires. *Phys. Rev. B* **46**, 3898–3905 (1992).
30. Mikhail, I. F. I. & Sayed, S. B. A. E. Exact and variational calculations of a hydrogenic impurity binding energy in a multilayered spherical quantum dot. *Physica E* **43**, 1371–1378 (2011).
31. Montenegro, N. P. & Merchancano, S. T. P. Hydrogenic impurities in GaAs-(Ga,Al)As quantum dots. *Phys. Rev. B* **46**, 9780–9783 (1992).
32. Xiao, Z., Zhu, J. & He, F. Magnetic field dependence of the binding energy of a hydrogenic impurity in a spherical quantum dot. *J. Appl. Phys.* **79**, 9181–9187 (1996).
33. Sahoo, S., Lin, Y. C. & Ho, Y. K. Quantum-confined hydrogenic impurity in a spherical quantum dot under the inuence of parallel electric and magnetic fields. *Physica E* **40**, 3107–3114 (2008).
34. Li, G., Branis, S. V. & Bajaj, K. K. Hydrogenic donor states in quantum dots in the presence of a magnetic field. *Phys. Rev. B* **47**, 15735–15740 (1993).
35. Aktas, S. & Boz, F. K. The binding energy of hydrogenic impurity in multilayered spherical quantum dot. *Physica E* **40**, 753–758 (2008).
36. Lin, M.-C. & Chuu, D.-S. Whittaker function approach to determine the impurity energy levels of coated quantum dots. *J. Appl.Phys.* **90**, 2886–2891 (2001).
37. Ham, H. & Spector, H. N. Photoionization cross section of hydrogenic impurities in spherical quantum dots. *J. Appl. Phys.* **93**, 3900–3905 (2003).
38. Zhu, J.-L. & Chen, X. Spectrum and binding of an off-center donor in a spherical quantum dot. *Phys. Rev. B* **50**, 4497–4502.
39. Ates, S. *et al.* Non-resonant dot–cavity coupling and its potential for resonant single-quantum-dot spectroscopy. *Nature Photonics* **3**, 724–728 (2009).
40. Fuechsle, M. *et al.* Spectroscopy of few-electron single-crystal silicon quantum dots. *Nature Nanotechnol.* **5**, 502–505 (2010).
41. Cui, J., Beyler, A. P., Bischof, T. S., Wilson, M. W. & Bawendi, M. G. Deconstructing the photon stream from single nanocrystals: From binning to correlation. *Chem. Soc. Rev.* **43**, 1287–1310 (2014).
42. Leonov, M. Y. *et al.* Transient intraband absorption of light by semiconductor nanorods. *J. Opt. Technol.* **80**, 648–654 (2013).
43. Leonov, M. Y., Turkov, V. K., Rukhlenko, I. D. & Fedorov, A. V. Kinetics of resonance luminescence of a single quantum dot at room temperature. *Opt. Spectrosc.* **113**, 265–270 (2012).
44. Rukhlenko, I. D. *et al.* Kinetics of pulse-induced photoluminescence from a semiconductor quantum dot. *Opt. Express* **20**, 27612–27635 (2012).
45. Leonov, M. Y., Turkov, V. K., Rukhlenko, I. D. & Fedorov, A. V. Kinetics of thermalized luminescence of a single quantum dot at room temperature. *Opt. Spectrosc.* **113**, 259–264 (2012).
46. Fedorov, A. V. & Rukhlenko, I. D. Study of electronic dynamics of quantum dots using resonant photoluminescence technique. *Opt. Spectrosc.* **100**, 716–723 (2006).

47. Landau, L. D. & Lifshitz, L. M. *Quantum Mechanics* (Pergamon, Oxford, 1977).
48. Baimuratov, A. S., Baranov, A. V. & Fedorov, A. V. Light absorption involving longitudinal optical phonons in semiconductor quantum dots. *Opt. Spectrosc.* **111**, 51–60 (2011).
49. Fedorov, A. V., Baranov, A. V. & Masumoto, Y. Acoustic phonon problem in nanocrystal–dielectric matrix systems. *Solid State Commun.* **122**, 139–144 (2002).
50. Fedorov, A. V., Baranov, A. V., Itoh, A. & Masumoto, Y. Renormalization of energy spectrum of quantum dots under vibrational resonance conditions. *Semiconductors* **35**, 1390 (2001).
51. Fedorov, A. V., Baranov, A. V. & Inoue, K. Exciton–phonon coupling in semiconductor quantum dots: Resonant Raman scattering. *Phys. Rev. B* **56**, 7491 (1997).
52. Luther, J. M., Jain, P. K., Ewers, T. & Alivisatos, A. P. Localized surface plasmon resonances arising from free carriers in doped quantum dots. *Nat. Mater.* **10**, 361–366 (2011).
53. Ellingson, R. J. *et al.* Highly efficient multiple exciton generation in colloidal PbSe and PbS quantum dots. *Nano Lett.* **5**, 865–871 (2005).
54. Empedocles, S. A. & Bawendi, M. G. Quantum-confined stark effect in single CdSe nanocrystallite quantum dots. *Science* **278**, 2114–2117 (1997).
55. Rukhlenko, I. D. *et al.* Spontaneous emission of guided polaritons by quantum dot coupled to metallic nanowire: Beyond the dipole approximation. *Opt. Express* **17**, 17570–17581 (2009).
56. Fedorov, A. V., Baranov, A. V., Rukhlenko, I. D., Perova, T. S. & Berwick, K. Quantum dot energy relaxation mediated by plasmon emission in doped covalent semiconductor heterostructures. *Phys. Rev. B* **76**, 045332 (2007).
57. Rukhlenko, I. D. & Fedorov, A. V. Penetration of electric fields induced by surface phonon modes into the layers of a semiconductor heterostructure. *Opt. Spectrosc.* **101**, 253–264 (2006).
58. Rukhlenko, I. D. & Fedorov, A. V. Propagation of electric fields induced by optical phonons in semiconductor heterostructures. *Opt. Spectrosc.* **100**, 238–244 (2006).
59. Fedorov, A. V., Baranov, A. V., Rukhlenko, I. D. & Gaponenko, S. V. Enhanced intraband carrier relaxation in quantum dots due to the effect of plasmon–LO-phonon density of states in doped heterostructures. *Phys. Rev. B* **71**, 195310 (2005).
60. Baranov, A. V., Fedorov, A. V., Rukhlenko, I. D. & Masumoto, Y. Intraband carrier relaxation in quantum dots embedded in doped heterostructures. *Phys. Rev. B* **68**, 205318 (2003).
61. Rukhlenko, I. D., Fedorov, A. V., Baymuratov, A. S. & Premaratne, M. Theory of quasi-elastic secondary emission from a quantum dot in the regime of vibrational resonance. *Opt. Express* **19**, 15461–15482 (2011).
62. Preisler, V. *et al.* Hole–LO phonon interaction in InAs/GaAs quantum dots. *Phys. Rev. B* **72**, 115309 (2005).
63. Zhao, J., Kanno, A., Ikezawa, M. & Masumoto, Y. Longitudinal optical phonons in the excited state of CuBr quantum dots. *Phys. Rev. B* **68**, 113305 (2003).
64. Fedorov, A. V. & Baranov, A. V. Exciton–vibrational interaction of the Fröhlich type in quasi-zero-size systems. *J. Exp. Theor. Phys.* **83**, 610–618 (1996).
65. Itoh, T. *et al.* Polaron and exciton–phonon complexes in CuCl nanocrystals. *Phys. Rev. Lett.* **74**, 1645–1648 (1995).
66. Abramowitz, M. & Stegun, I. A. (eds.). *Handbook of Mathematical Functions* (Dover, New York, 1965).
67. Madelung, O., Schultz, M. &Weiss, H. (eds.). *Landolt-Börnstein, New Series, Group III,* 1th edn, vol. 17, Pt. a (Springer-Verlag, Berlin, 1982).


## Acknowledgments

The authors gratefully acknowledge financial support from the Ministry of Education and Science of the Russian Federation through its Grant Nos. 3.17.2014/K and 14.B25.31.0002. The Ministry of Education and Science of the Russian Federation also supports A.S.B. and M.Yu.L., through its scholarships of the President of the Russian Federation for young scientists and graduate students (2013–2015). A.S.B. gratefully acknowledges the Dynasty Foundation Support Program for Physicists. The work of I.D.R. is funded by the Australian Research Council, through its Discovery Early Career Researcher Award DE120100055. I.D.R. and A.S.B. also gratefully acknowledge the financial support from the Monash Researcher Accelerator Program.

## Author contributions

I.D.R., A.V.B. and A.V.F. jointly suggested the study conducted by A.S.B., V.K.T., M.Yu.L. and I.O.P. Namely, A.S.B., V.K.T., M.Yu.L. and I.O.P. performed analytical calculations and analyzed the obtained expressions, drew the figures, and prepared the first draft of the manuscript. I.D.R., A.V.B., T.S.P., K.B. and A.V.F. supervised the study, contributed to the analysis and interpretation of the results, helped to formulate and present the research outcomes, and thoroughly edited the manuscript.

## Additional information

**Competing financial interests:** The authors declare no competing financial interests.

**How to cite this article:** Baimuratov, A.S. *et al.* Level Anticrossing of Impurity States in Semiconductor Nanocrystals. *Sci. Rep.* **4**, 6917; DOI:10.1038/srep06917 (2014).